



Development of a customised 3D printer as a potential tool for direct printing of patient-specific facial prosthesis

Cormac D. Fay^{1,2} · Ali Jeiranikhameneh² · Sepidar Sayyar^{2,3} · Sepehr Talebian² · Alex Nagle² · Kai Cheng⁴ · Sophie Fleming⁵ · Payal Mukherjee⁴ · Gordon G. Wallace²

Received: 18 February 2022 / Accepted: 3 April 2022 / Published online: 22 April 2022
© The Author(s) 2022

Abstract

This study demonstrates a cost-effective portable fabrication system for 3D printing complex structures from polydimethylsiloxane (PDMS). Material development and characterisation allowed for the design and production of a 3D printer that is capable of fabricating PDMS structures using a photo-initiator and a LED curing process. A 3D model of a participant's ear was captured using a handheld scanner. These data were used to directly 3D print an ear. Micro-extrusion direct deposition of PDMS at room temperature is demonstrated via a custom designed 3D printer, with in situ UV cross-linking to facilitate curing of the PDMS during the 3D printing process. This 3D printer has great potential to be used as a fast and facile fabrication approach to create facial and other prosthesis. Future developments will also focus on other application areas such as microfluidics, flexible electronics, and other biomedical applications.

Keywords Silicone · Prosthesis · Ear · 3D printing · Photo cross-linking · 3D scan

1 Introduction

Microtia–anotia is a congenital birth deformity where the external ear (pinna) framework is either underdeveloped or completely absent [1, 2], which affects approximately one in every 5,000 births worldwide [3, 4]. Treatment of this is largely classified into surgical reconstruction and external prostheses. For the majority of cases, the typical treatment

is prosthetic reconstruction—with the aim of restoring the aesthetic shape of the natural ear [5]. This approach offers a less invasive, and often more aesthetical and symmetrical alternative to reconstructive surgery [6]. Prosthetic rehabilitation is especially viable for regions and individuals without access to reconstructive surgical facilities and/or for those unable to undergo surgical intervention [7].

The art of making cranio-facial prostheses is known as anaplastology. Historically, a number of materials have been used for this purpose [8, 9], for example porcelain, polyethylene, wax, rubber, and papier-mâché [9–12]. A breakthrough material came in the form of modern silicones, with enhanced simulation of skin characteristics in terms of their flexibility, pigmentation, ability to be cast at room temperature, hardness, and tensile strength [13, 14]. Fabrication of prosthetics continues to be dominated by operator-dependent casting methods [15]. There are good reasons for this approach, as the prosthesis must adhere to the nuances and complexities of the user and often goes through refinements, requiring a considerable labour investment of up to 14 hours for an ear prosthesis [7, 13, 16]. To address this, the past decade has gradually seen an increase in the adoption of Computer-Aided Design/Manufacturing (CAD/CAM) technologies for prosthesis development as recently reviewed by Mussi et al. [17] and Manero et al. [18]. Notwithstanding

✉ Gordon G. Wallace
gwallace@uow.edu.au

¹ SMART Infrastructure Facility, Engineering and Information Sciences, University of Wollongong, Northfield Avenue, Wollongong 2522, NSW, Australia

² ARC Centre of Excellence for Electromaterials Science (ACES), Intelligent Polymer Research Institute (IPRI), AIIM Facility, University of Wollongong, Northfield Avenue, Wollongong 2500, NSW, Australia

³ Australian National Fabrication Facility & Materials Node, Intelligent Polymer Research Institute (IPRI), AIIM Facility, University of Wollongong, Northfield Avenue, Wollongong 2500, NSW, Australia

⁴ Prosthetic Art Technology Pty Ltd., 2/2 High Street, Alstonville 2477, NSW, Australia

⁵ Royal Prince Alfred Institute of Academic Surgery, Sydney Local Health District, Sydney 2050, NSW, Australia

the impact of such tools, the majority of reviewed studies involved the printing of moulds for prosthetic fabrication [19], with relatively little or no attention given to printing of silicones in this area.

Eggbeer et al. categorized additive fabrication of silicone structures into two approaches, i.e. direct and indirect [20], with the majority of studies in other domains focusing on the indirect approach which involves printing moulds followed by conventional casting [21–25]. The majority of prosthesis production also follows the indirect mould-cast method [17]. One reason for this is due to the inherent challenges faced when using highly viscous, non-Newtonian materials such as different silicone types (e.g. UV or thermal cross-linkable) [26], which have an impact over many additive manufacturing techniques, e.g. the maximum viscosities found for SLA were in the range of 300–5,000 mPa.s [27] and 10–100 mPa.s for drop-on-demand inkjet printing [28, 29]. However, extrusion-based dispensing has been reported to successfully dispense materials with viscosities ranging from 30 – 6×10^7 mPa.s [28, 30]. Recently, Ross et al. [31] reviewed the use of 3D printing approaches for aesthetic reconstruction of microtia, discussing studies involving direct printing of materials. Mohammed et al. [32] investigated the use of commercially available equipment (Connex 3 500) and their proprietary material, Tango Plus (not silicone), to produce a 3D printed ear from CT scans. The company Picsima proposed a system capable of printing silicone; however, this required a complexity of printing within a bath composed of a silicon oil in addition to a cross-linker, with Cartesian controlled extrusion of a catalyst and a post-cleaning process (picsima.com). Based on this account and others reviewed by Ross et al. [31], there does not appear to be a reported study in the literature involving direct free standing 3D printing of silicone ear shapes using micro-extrusion technique. The closest study using PDMS and micro-extrusions for printing ears was by Mannoor et al. [33], but for tissue engineering purposes not prosthesis.

An important step prior to the use of 3D printing of prosthesis is capturing the data needed to create the required customised structure. Reviews of 3D scanning technology in this area show that they are mostly based on sophisticated instrumentation available in centralised facilities [34], e.g. via CT or MRI as discussed previously [32]. Access to this equipment, along with highly trained personnel and processing softwares, is prohibitively expensive. More recently, hand held scanners have emerged offering a solution in terms of portability and lower cost compared to MRI or CT approaches. These are lower in price (\$25k–\$100k), portable and offer an alternative solution to 3D imaging in comparison with MRI or CT technologies that are unlikely to be available in underdeveloped regions.

While there have been reports of using conventional 3D printers for facial prosthesis, such as nasal [35], a focus on

colour production [36], or printing in other materials such as wax [37], the use of this technology primarily focuses on the cast and moulding approach [38–41]. Based on the above accounts, there has been no reported study proposing an approach capable of 3D printing free standing silicone-based complex structures, namely an ear shape, via micro-extrusion in a portable and cost-effective manner. In other words, one effectively priced for widespread deployments, for less than \$1,000 USD component cost. Although there are some reports on the development of custom made and low cost additive manufacturing (AM) equipment for other AM technologies [42–47] that can make use of emerging novel materials [48], this study demonstrates, for the first time, an approach capable of scanning an individual's ear using a handheld scanner, mirroring it in virtual space, and reproducing its symmetrical counterpart in PDMS using a low-cost, ad hoc 3D printer to suit the high viscosity of the material. Development and characterisation of the PDMS material used is presented, which informs the design of the ad hoc 3D printer. Scanning of a participant's ear, processing of the model, and production via the printer is proposed. All of which will be explored using freely available or open-source softwares to enhance the cost-effectiveness of the proposed solution.

2 Experimental

2.1 System design

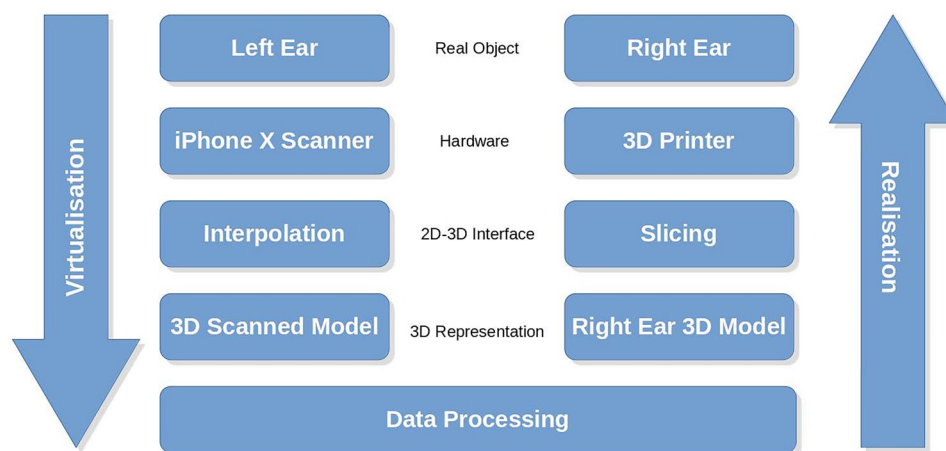
Other studies [31, 49] have proposed a high-level framework for the production of organs/prosthesis from 3D scanning to 3D printing. An adapted version of this is shown in Fig. 1, which demonstrates the model adopted in this study. A patient's left ear is scanned by an EinScan Pro 2X Plus portable Scanner where it develops a 3D model via progressive 2D depth data streams and produces a 3D representation of the craniofacial area of the participant. Data processing allows for extraction of the ear data, which is virtually mirrored to produce a symmetric model of the patient's right ear. The 3D model is sliced into 2D layers (a symmetry in the scanning process) and sent to the developed 3D printer for realisation of a symmetrical right ear prosthetic for the patient.

2.2 Materials & characterisation

2.2.1 Material preparation

To prepare the printing ink, the base material (prepolymer) and catalyst (Silopren UV LSR 2030, Momentive) were added into a container in a 100:2 ratio (based on the material datasheet) followed by the addition of the silicone-based

Fig. 1 Framework adopted in this study to 3D print a right ear shape from scanning of a patient's left ear



thixotropic agent (TA) (sil-thix silicone thickener - Barnes) at two different concentrations (0.05 and 0.1 wt.%). The combination was mixed through a planetary centrifugal mixer (THINKY Mixer ARE-310) until a uniform mixture was formed. The samples were labelled as PDMS-0, PDMS-0.05, and PDMS-0.1, according to the weight percentage of the agent (e.g. PDMS-0.1 contains 0.1 wt% TA). Material preparation and 3D printing were performed in a temperature and humidity controlled laboratory set to 22 °C and 59%, respectively, using a Liebert PEX Precision Air Conditioning system - VERTIV.

2.2.2 Rheology & cross-linking kinetics

Rheological properties were measured using an AR-G2 rheometer (TA Instruments). Viscosity measurements were carried out using a cone plate (20 mm diameter and 2° cone angle) geometry. Photorheological characterization was performed at a frequency of 1 Hz and 1% strain, both in the linear viscoelastic range, using a 20 mm parallel plate geometry. UV irradiation was applied using an optics attachment and an OmniCure® S1000 as the light source.

2.3 3D printer development

Figure 2 presents the design of the printer using 3D CAD software (FreeCAD, 1.8.4). Four (4) linear modules (RobotDigg, SHF1-Z) were sourced and arranged to allow for the 3D translational movements—denoted as standard as X, Y and Z (1 & 2). The Z-axis was designed in a gantry style with two linear stages (as shown in the figure) in order to support the weight of the Y-axis and an additional load of the strong extrusion mechanism. The X-Axis is detailed to show the linear movement of all four axes, i.e. via a lead screw (2 mm pitch), coupler, two guide rails, carriage and a stepper motor (NEMA 17, 1.33 A, 0.9°/step, RobotDigg 42HM60-1684). The print base was attached to the x-axis

carriage, which accommodated a petri dish and was adjustable via three (3) levelling screw-spring combinations to ensure that the print base was in line with the 3D movements of the axes.

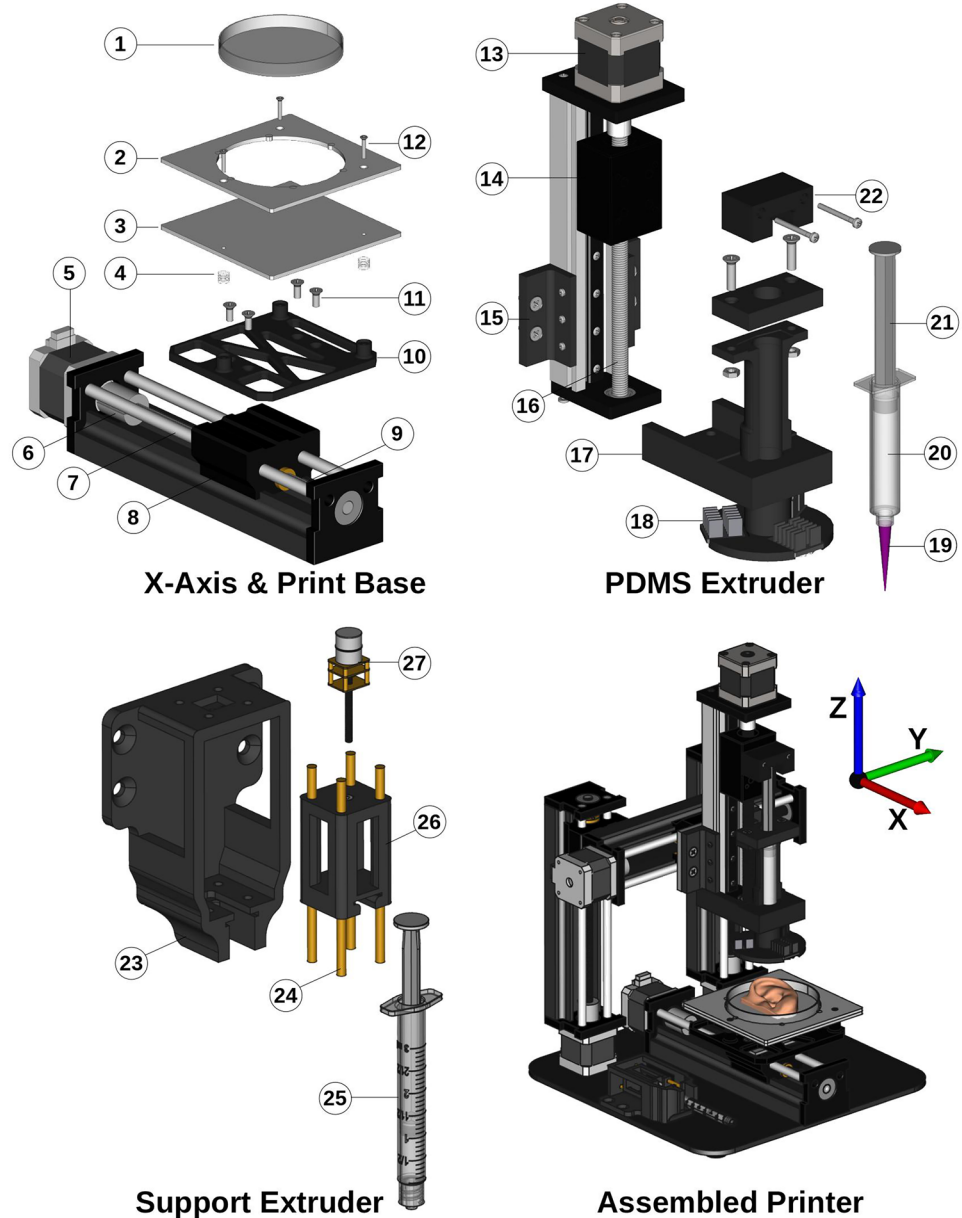
The PDMS extrusion mechanism consisted of a hardened steel frame with movement via a MGN12 linear rail (RobotDigg 200_WL_89), which was driven by a high torque motor (Nema 17, 2.5 A, 1.8°/step, RobotDigg 42HS48-2504). This was designed to achieve extrusion of the PDMS after material characterisation took place. Additional components were designed and attached to the extrusion mechanism to accommodate a standard 10 ml syringe equipped with a conical tip (SmoothFlow, Nordson). Three emitter modules were located 120° apart at the base of the extrusion mechanism to ensure irradiation of the extruded PDMS in-line and from multiple surrounding angles during printing. Each emitter module consisted of a high power 365 nm LED module (LedEngin Inc, LZ4-44UV00-0000) attached to a 12.2 K/W heat sink (Aavid Thermalloy, 6238PB-MT5) to dissipate the heat generated by the LED.

Considering the geometric complexity of target prints, i.e. ears, it was necessary to implement a support material extrusion system to enable features such as overhangs (amongst others) necessary for ear-shaped printed features. The support material extrusion mechanism was designed to accommodate a compatible material (Nordson, 7016093) dispensed from a 3 mm syringe and capable of non-adherence to the PDMS in addition for it to be washed away post print. A geared step-up motor (Fixer3D) was sourced that allows for a linear movement of the carriage resulting in controlled extrusion of the syringe. This took place via holding the syringe bung in the carriage and the flange by the frame. A length of 3 mm tubing was affixed from the syringe outlet to a nozzle mounted at the same height as the PDMS tip, but offset in the -Y direction by 50 mm.

The dynamics of the system was controlled via a logic control board (Arduino Mega 2560) flashed with open

Fig. 2 CAD drawings of the 3D Printer design and assembly.

(1) Petri dish. (2) Dish holder—upper. (3) Dish holder—base. (4) Spring. (5) Axis motor. (6) Coupler. (7) Guide rail. (8) Carriage. (9) Lead screw. (10) Print base mount. (11) M5 retention screw. (12) Dish holder retention screw. (13) Extrusion motor. (14) Carriage. (15) Extrusion mechanism mount. (16) Extrusion lead screw. (17) Syringe and emitter mount. (18) UV light emitter module. (19) Conical syringe tip. (20) Syringe barrel. (21) Syringe plunger. (22) Plunger flange retainer. (23) Support extruder frame. (24) Carriage guiding rails. (25) Syringe. (26) Carriage. (27) Step up geared motor



source firmware (Marlin 1.1) and connected to an outbreak board (Ultimaker, 1.5.7) designed with peripherals for 3D printers. Control of each axis motor (XYZ and the extruder) was achieved via stepper motor drivers (RobotDigg, TMC2100) with micro-stepping enabled ($n = 16$). Power to each LED was via three high current DC-DC step down regulators (Duinotech, XC-4514) and a single I/O on the microcontroller. The base firmware was altered to accommodate the correct board, steps/mm ratio (discussed next) and customised M codes (machine [customised] action codes within the G-Code framework) to control the LEDs. The 3D CAD model was sliced using third party software (Slic3r), which resulted in G-Code based on the print settings, see Table 1. Open source software (MatterControl 1.7.5) was

used to control the print operation by sending the resulting G/M-Codes to the printer over a USB connection.

Considering that a 2 mm pitch lead screw was used and connected to a $0.9^\circ/\text{step}$ stepper motor, the movement resolution is calculated by Eq. 1. With microstepping enabled ($n = 16$), it can be shown that a Step/mm ratio of 3,200 ($200\text{Steps} \times 16$) will allow the firmware to accurately control the axes movements. In order to verify this, a calibration routine took place whereby the axes were set to move a desired/theoretical distance and then measured using digital vernier calipers. This approach was adopted for two ranges, i.e. 0–100 mm and 0–10 mm. However, it was not possible to use the calipers to measure below this range. For this, an interferometer (Panasonic, HG-C1050-P) was employed

Table 1 Printing parameters

Parameter	Value	Unit
Print Speed (XYZ movement)	5	$mm.s^{-1}$
Syringe Size	10	cc
XYZ Motor Driver Control	600	mV
Microstep Resolution	16	steps
Layer Height	0.6	mm
Extrusion Feed Rate	40	$\mu L.s^{-1}$
Retraction Distance	4	mm
Retraction Speed	3	$mm.s^{-1}$
Layer to LED Distance	50	mm
LED Irradiance	25	$W.cm^{-2}$
Tip diameter/Layer Height	580	μm
Room Temperature	22	$^{\circ}C$

by affixing it onto the axis and using infrared reflectance to ascertain the resolution on the micron range from 0 to 1 mm and 0 to 100 μm .

$$\begin{aligned}
 1 \text{ revolution} &= 360^{\circ} = 2 \text{ mm} \\
 360^{\circ}/0.9^{\circ} &= 400 \text{ steps/rev} \\
 1 \text{ step} &= 5 \mu m
 \end{aligned}
 \tag{1}$$

2.4 3D object capturing & data processing

Scanning was conducted using EinScan Pro 2X plus scanner (Shining 3D, Hangzhou, China) at a resolution of 0.3 mm. The scanned model was processed using EXScan Pro 3.3.0.3 software (Shining 3D, Hang-zhou, China) by removing irrelevant scanned models. The post-processed model was then exported to a .stl file. Meshmixer and Meshlab were used to further refine the model by filling small holes and optimizing the topology of the model.

2.5 Material characterisation

Developing an ink with suitable rheological properties is essential for 3D printing complex structures. The elasticity and viscosity of the ink should be high enough to form a structure without requiring a high extrusion force. A PDMS prepolymer has a low elasticity before cross-linking, meaning that it can barely retain its shape, which results in structural collapse during the printing process. The viscosity, elasticity, and consequently the printability, of the prepolymer can be improved through incorporating a small amount of a thixotropic polymer without damaging the inherent properties of PDMS. The viscosity of the inks (with 0, 0.05 and 0.1 wt.% TA) and their variation vs time was evaluated (Fig. 3a). The ink's viscosity could be tailored by varying the TA concentration. The

viscosity of the blank PDMS (0 wt.% TA) was around 490 Pa.s, which increased to ~ 860 and 1,200 Pa.s by the addition of 0.05 and 0.1 wt.% TA, respectively. There is not any significant variation in viscosity of the samples at a constant shear rate, indicating that the inks do not cross-link after the addition of the cross-linker and before UV exposure, which is favourable when printing UV-cross-linkable inks.

A printing ink is constantly under a shear force during extrusion printing, which can change its rheological properties temporarily or permanently. Investigating the rheological behaviour of the ink under shear is of importance in order to predict its behaviour during the printing. The viscosity of inks vs shear rate is demonstrated in Fig. 3b. All samples showed a shear thinning behaviour by increasing the shear rate, which is characteristic of non-Newtonian fluids. Ink samples containing TA exhibited a more prominent shear thinning behaviour starting at low shear rates. Shear thinning behaviour is essential for inks used in 3D printing as it ensures uniform ink extrusion and high print fidelity [50]. These results indicate that the viscosity can be modified by incorporating a small amount of TA to improve the printability of the ink. Furthermore, the TA could help the polymer chains to slide against each other more easily, so the ink could be extruded more uniformly. Based on our observations and material characterisation, the reliability of this result was supported during the printing optimisation phase. We found that inks containing TA can be extruded more easily and more uniformly. This observation is confirmed by the rheology results, as the ink samples containing TA exhibited a more prominent shear thinning behaviour starting at low shear rates, indicating uniform ink extrusion and high print fidelity, see Fig. 3b.

The cross-linking behaviour of the inks with different TA concentrations is demonstrated in Fig. 3c. In a PDMS ink with no TA content (PDMS-0), the magnitude of G'' (loss modulus) is higher than G' (storage modulus), indicating the liquid-like behaviour of the ink before cross-linking. Switching on the UV irradiation initiated the cross-linking followed by G' surpassing G'' after approximately 2 minutes. The modulus curves gradually levelled off over time due to the formation of the cross-linked structure.

The addition of TA significantly improved the elastic behaviour of the ink, as evident by G' values higher than G'' before UV exposure. Similar to the blank PDMS, the cross-linking was initiated in the PDMS inks containing TA shortly after UV exposure. The cross-linking rate and ultimate G' values in modified inks (PDMS-0.05 and PDMS-0.1) are comparable to blank PDMS, indicating that the addition of TA up to 0.1 wt.% has no significant effect on the cross-linking behaviour and ultimate elastic modulus of the sample (Fig. 3c). Based on the rheology and 3D

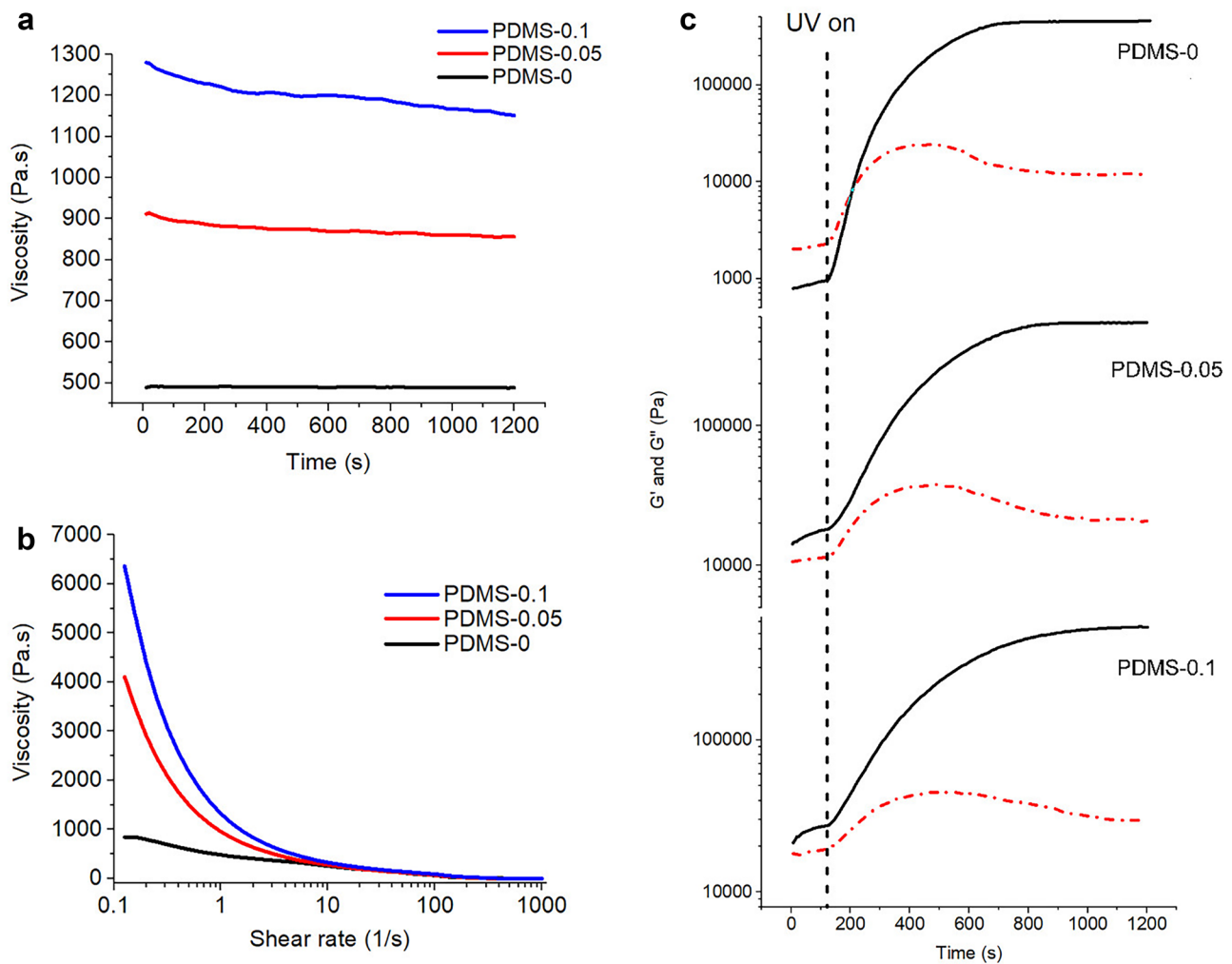


Fig. 3 Viscosity of PDMS inks vs (a) time and (b) shear rate. (c) Cross-linking kinetics of the PDMS inks with UV exposure beginning at 120 s. G' and G'' are represented with solid and dash-dot lines, respectively

printing optimisation results, PDMS-0.05 was found to be an appropriate formulation to 3D print complex structures with our 3D printer.

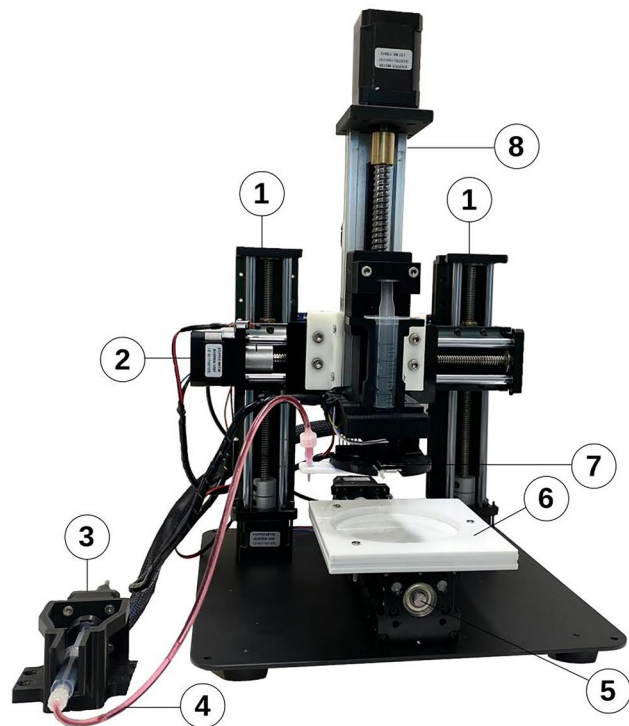
2.6 3D printing system

Figure 4 presents the realised developed printer as described previously via the design in Sect. 2.3 and presented in Fig. 2. Closer views of the printer components are also provided in addition to printing of the first layers of an ear taking place. Additionally, enlarged views are provided in the Supplementary Information. A tapered printing tip (SmoothFlow tapered tip, Nordson) was chosen to better suit extrusion of a viscous material over traditional tips available. Within this tip range, smaller diameters successfully extruded the material; however, due to the material's viscosity the motor driver began to overheat making it difficult to sustain for prolonged periods, e.g. for printing an ear shape. A $580 \mu\text{m}$

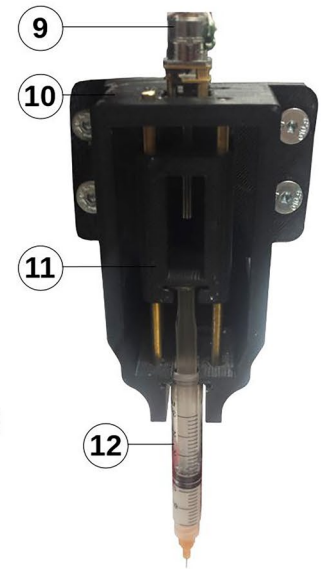
diameter tip was chosen for this reason. Surrounding the tip were three LED modules, as shown in the figure. This was to ensure that photo-cross-linking took place by surrounding the target area at multiple points as the material can trail at many angles, relative to the tip, during printing.

Figure 5(a–c) presents the calibration of the X, Y and Z in the 10 mm and 100 mm range. It can be seen that good linear fits result when comparing the desired (software) distance to the measured distance travelled of each axis. This demonstrates the reproducibility of the axes and their capability to print down to the 1 mm resolution range. However, in order to examine this more closely the movement was measured using an interferometer as described previously. Figure 5(d, e) demonstrates the resolution of the axes at the micron resolution. While theoretically the resolution is 312.5 nm (or 5 nm without microstepping), the interferometer was not sensitive enough to measure in that range. This is evident in Fig. 5e with the instrument rounding the distance to the nearest 10

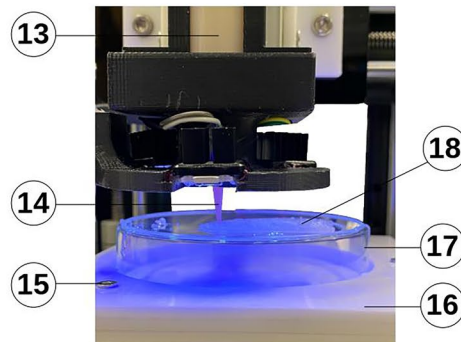
Fig. 4 Captured and labelled images of the developed printer: while printing an ear, the photo-initiation system and the extruders. (1) Z-Axis. (2) Y-Axis. (3) Support extruder. (4) Support material in tubing. (5) X-Axis. (6) Print support base. (7) Irradiation system. (8) PDMS extruder. (9) Support extruder motor. (10) Frame. (11) Carriage. (12) Support material syringe. (13) PDMS syringe. (14) Tip. (15) Levelling screw. (16) Dish support. (17) Petri dish. (18) Printing ear layers. (19) LEDs. (20) UV LED heat sink. (21) Extrusion motor. (22) Coupler. (23) Carriage. (24) Mounting brackets. (25) Syringe barrel. (26) Syringe plunger. (27) Bung holder/guide



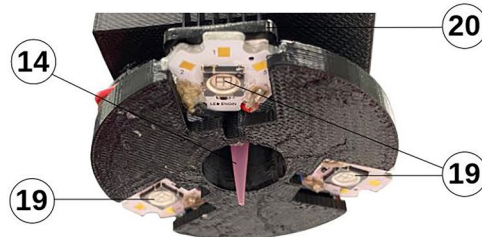
Assembled Printer



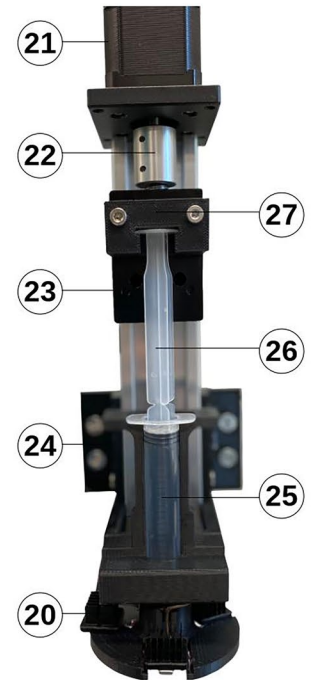
Support Extruder



Printing Layers



Irradiation System



PDMS Extruder

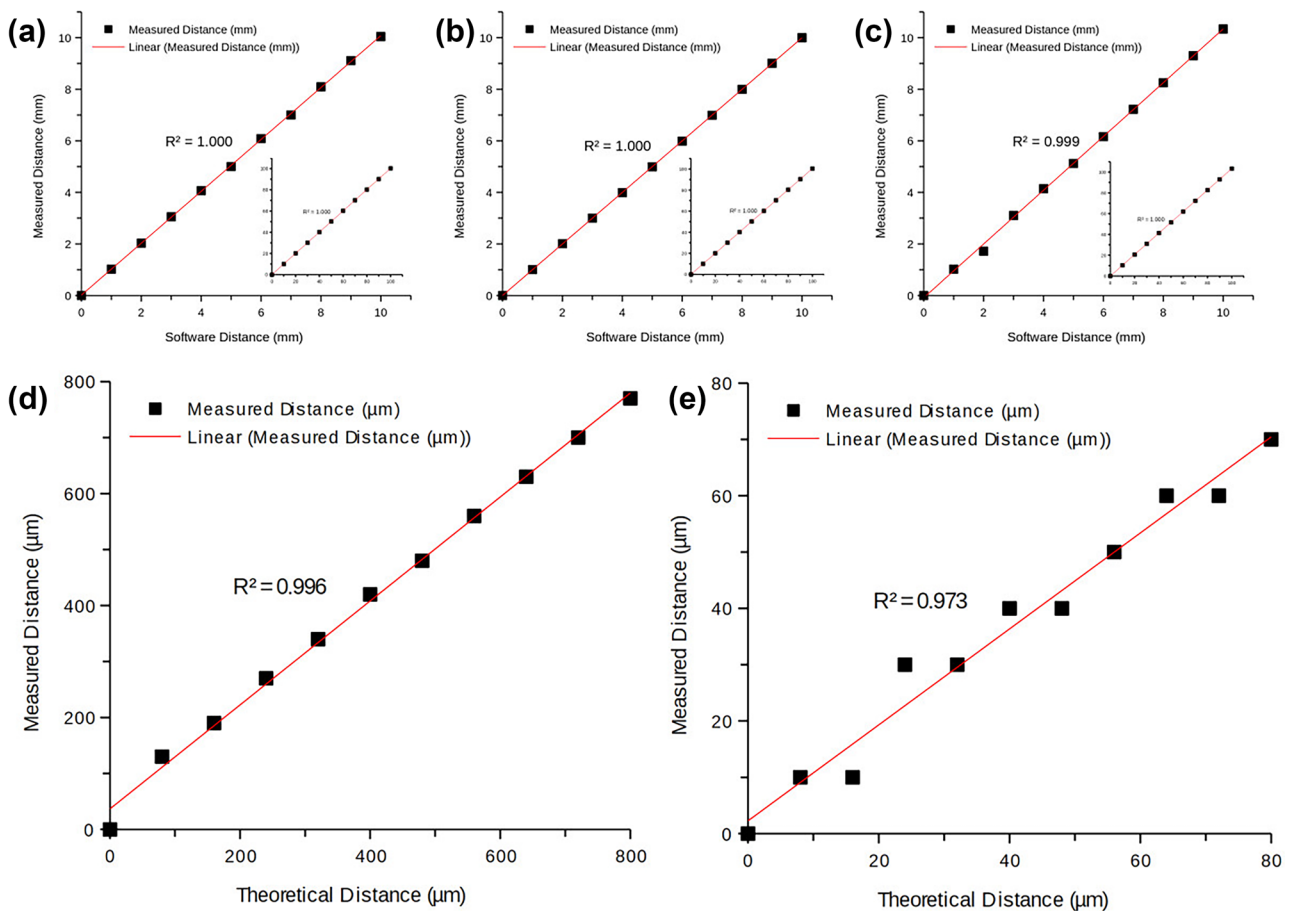


Fig. 5 (a–c) Calibration of the X, Y and Z axes from 0–10 mm and 0–100 mm (inset) using a 3,200 Steps/mm ratio. (d–e) Calibration of a single axis using an interferometer at different Steps/mm ratios to examine the resolution. Black squares represent the aver-

age of successive measurements ($n = 3$), error bars are the standard deviation (difficult to see due to the high reproducibility of the data). Red lines represent good linear fits: $R^2 > 0.99$, $n = 11$ for ‘a–d’ and $R^2 = 0.973$, $n = 11$ for ‘e’

μm increment. Regardless, this shows that the measured resolution was sufficient for the purposes of printing ear shapes.

2.7 3D printing an ear shape

MatterControl software was used to adjust the printing parameters and subsequently slice the captured ear STL file. Given the curvatures and overhangs of the ear model, support material (Vaseline, Petroleum Jelly) was used to further ensure the structural integrity of the printed part (Fig. 6). Also, the three UV LEDs equipped on the printer were continuously exposing the part to radiation throughout the entire printing process. After the printing was done, the part was further exposed to UV radiation for an extra 5 min to ensure sufficient cross-linking of the top layers. This was followed by removing the support material and cleaning the part with soap and water to wash the excess Vaseline.

To evaluate the print accuracy, different areas of the 3D printed ear were observed under a microscope and compared

with the STL file (Fig. 6). This was achieved through the microscope’s software tool set that allowed for measurement of the total dimension, line spacing, strut size and layer height. The printed ear part had comparable dimensions ($33.6\text{mm} \times 28.9\text{mm} \times 63.4\text{mm}$) to that of the ear STL model ($34.9\text{mm} \times 29.9\text{mm} \times 61.6\text{mm}$). This small deviation from the original dimensions could be attributed to the infill density of the printed ears. Changing of the infill density is associated with reducing the line spacing, this in turn will lead to further diffusion of neighbouring layers which can affect geometric fidelity and spatial resolution. Microscopy images of the printed ear further revealed the layer height of these structures (0.58 ± 0.1 mm) as compared to the set printing value in the software (0.5 mm). This could be a result of multiple factors such as layer diffusion, die swelling of the PDMS upon extrusion, and nozzle movement speed during printing. The 3D printing procedure was optimised to minimise the defects and die swelling; however, some degrees of die swelling (i.e. an increase in diameter

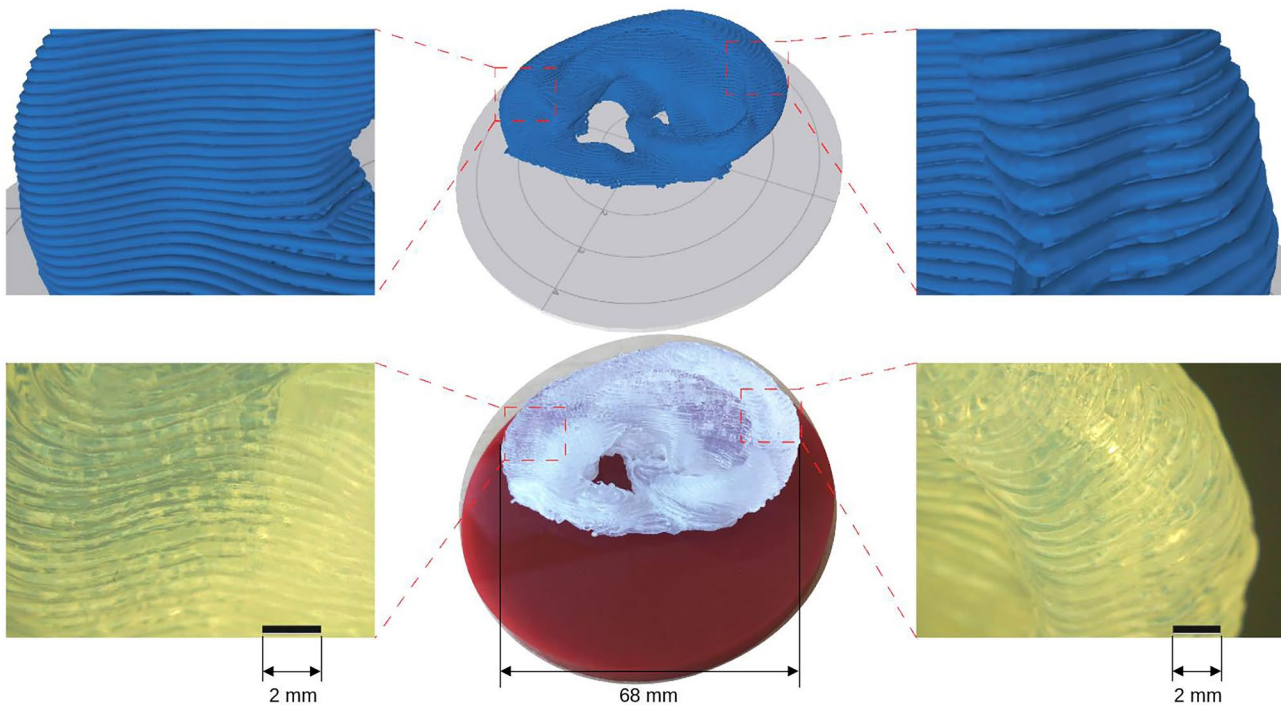


Fig. 6 Depicting sliced STL model of the ear (top row), and the corresponding 3D printed ear (bottom row)

of the extruded struts due to elasticity of the material) are inevitable during the printing. Microscopy images of the printed ear further revealed the layer height of these structures (0.58 ± 0.1 mm) as compared to the set printing value in the software (0.5 mm). This could be a result of multiple factors such as layer diffusion, die swelling of the PDMS upon extrusion, and nozzle movement speed during printing. Overall, the printed ear showed close resemblance to the STL model, and the overhanging areas and curvatures were successfully fulfilled by the printer. This was due to the ears being printed using the optimised printing condition, which were inspected under microscope for defects. No observable structural defects were noticed.

The mechanical recoverability of the 3D printed ear was examined by subjecting it to 100 cycles of a cyclic compression test with up to 70% strain. A large hysteresis loop and decline of the stress value are undesirable as it indicates deformation of a sample [51]. The 3D printed ear showed a small hysteresis loop and stress decline over the 100 loading-unloading cycles when compressed up to 70% strain, see Fig. 7a. The shape and volume of the 3D printed ear remained almost the same after 100 cycles of compression with no apparent variation compared to the original sample (Fig. 7b). These results indicate that the 3D printed ear can endure a large force with minimal deformation and no fracture.

To further investigate the mechanical properties of the printed structures, a standard dog-bone shape was 3D printed using the PDMS in order to measure its tensile strength and

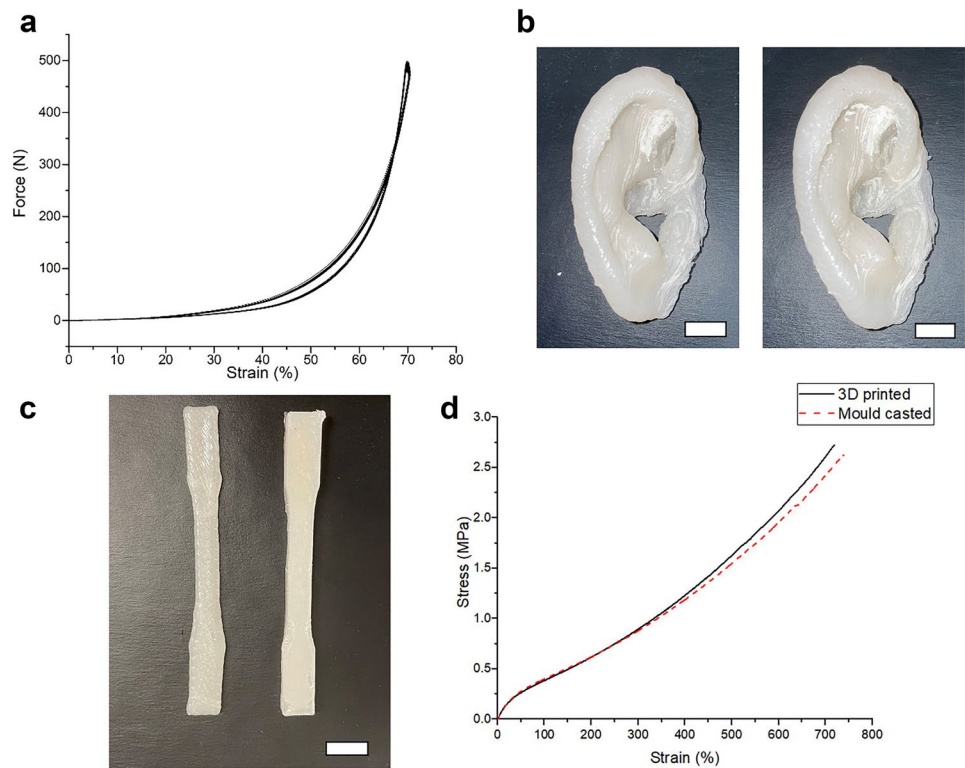
strain at break. Dog-bone shape samples were also prepared through mould casting for comparison (Fig. 7c). 3D printed and mould-casted samples exhibited similar stress/strain curves, tensile strength and strain at break values, implying that the mechanical properties of the 3D printed structure is comparable to the mould-casted sample with no structural defects introduced by 3D printing (Fig. 7d).

2.8 Further discussions

One of the primary advantages of the developed solution is its portability and cost effectiveness. The developed printer is very compact and capable of being transported to a number of locations including within clinical environments and/or developing regions. This has the capacity to impact regions without access to centralised healthcare facilities to develop patient-specific prosthesis. The cost effectiveness of this printer is relatively high, and as a mobile platform it can immediately impact developing regions, allowing for mobile clinics to access this cheaply and quickly. A breakdown of costs is shown in Table 2, with a low total cost of ca. \$625.

There are a number of other opportunities to examine. Considering that medical grade silicones are available for printing, other supracutaneous craniofacial prosthesis/structures that currently require ad hoc manufacturing are targeted for investigation, e.g. nose [52, 53]. Moreover, flexible subdermal structures required as a result of physical trauma or congenital disfigurement will be considered. In order for

Fig. 7 (a) Cyclic compression test of 100 cycles up to 70% strain of the printed ear. (b) Captured images of the printed ears before (left) and after (right) cyclical compression tests. (c) Printed (left) and moulded (right) dog bone shapes. (d) Tensile tests of the dog bone structures. Scale bars represent 1 cm



a prosthesis to successfully alleviate the emotional suffering of patients, it must be realistic in appearance [54]. On that basis, another avenue for progression will be in the automatic colouring of the silicone during printing [36]. Printing in the natural pigmentation colour of a patient's skin is an important feature to possess for future consideration.

Facial prostheses are required to possess good mechanical properties and high durability as they are under tension by the users during the daily cares. Therefore, investigating the mechanical properties of the fabricated prostheses is of great importance. Compression of the 3D printed ear in cycles can mimic the tensions applied to the ear by the users in real life condition. In this work, we subjected the

3D printed ear to 100 cycles of a cyclic compression test with up to 70% strain. The ear showed a very negligible deformation after 100 cycles of compression, indicating that the 3D printed ear has a very low defect and a very high durability. The result implies that our system is suitable for fabricating facial prosthesis. To the best of our knowledge, it is the first time that such an experiment is performed on a prosthetic ear. Other mechanical properties tests such as impact and indentation tests can provide more information in this regard. Having appropriate viscosity and elasticity is a necessity for a printing ink to ensure fabricating high-resolution structures. Materials with low viscosity cannot hold their shape after printing, while high viscous materials are hard to extrude. We demonstrated that the viscosity, elasticity, and shear thinning behaviour of the ink can be tailored through utilising a small amount of a silicone thickener to make the ink more suitable for printing high-resolution structures. Further optimisation of the rheological properties of the ink should lead to higher fidelity printing.

Table 2 Breakdown of component costs for the developed fabrication system

Component	Cost (US\$)
Axes & Motors x4	89
Logic Board & Drivers	125.57
Extrusion Rail	60
3D Printed Components	120
LEDs x3	157.7
Heatsink	5.97
Regulators x3	18.73
Lab Consumables	50
Total	626.97

3 Conclusions

We developed a user-friendly, portable and low-cost 3D printing system (~\$625 USD, component cost) for direct 3D printing of a mirrored ear shape fabricated in silicone. By using a handheld scanner and open source software combined, we could 3D print silicone-based ear shapes

in different sizes with good resolution. Although this system aims to restore the aesthetic shape of the natural ear for 3D printing facial prosthetics, it offers high potential to 3D print many other types of bodily shapes through minor hardware modifications. This technology holds the potential for patients to be provided with an appropriate prosthesis in a single clinical visit within a few hours—a considerable reduction from a prosthetist's labour investment of ca. 14 hours (impacting costs) for an ear prosthesis. The viscosity of the PDMS could be tailored through adding a slight amount of a thixotropic agent to improve the printing fidelity without altering the inherent properties of the polymer. This means that the other external (or indeed internal) features can be fabricated in a similar fashion, e.g. nose, in addition to matching the ink's colour with the patient's skin tone.

In summary, the findings of this work are:

- **Silicone:** Formation and characterisation of a PDMS-based silicone-based ink for additive manufacturing purposes.
- **3D Printer:** Design and Development of a low-cost customised 3D Printer capable of printing silicone structures in a layer-by-layer fashion.
- **Printing Method:** Creation of a silicone printing method whereby a layer is first deposited and photo-initiated while printing.
- **Prosthetic potential:** We applied this technique to produce an anatomically accurate mirror image ear model from a scan of a participant's opposing ear in a timely manner.
- **Print Characterisation:** We performed characterisation of the printed silicone ear, which showed considerable robustness making it ideal as a wearable prosthetic for use.

Supplementary Information The online version contains supplementary material available at <https://doi.org/10.1007/s00170-022-09194-0>.

Author contributions All authors contributed to the study conception and design. Material preparation, data collection and analysis were performed by Cormac D. Fay, Ali Jeiranikhameneh, Sepidar Sayyar, Sepehr Talebian, Alex Nagle, and Kai Cheng. The first draft of the manuscript was written by Cormac D. Fay, and all authors commented on previous versions of the manuscript. All authors read and approved the final manuscript.

Funding Open Access funding enabled and organized by CAUL and its Member Institutions. The authors wish to acknowledge funding from the Australian Research Council (ARC) Centre of Excellence Scheme (CE140100012) and support from the Australian National Fabrication Facility (ANFF) - Materials Node.

Declarations

Competing interests The authors have no relevant financial or non-financial interests to disclose.

Open Access This article is licensed under a Creative Commons Attribution 4.0 International License, which permits use, sharing, adaptation, distribution and reproduction in any medium or format, as long as you give appropriate credit to the original author(s) and the source, provide a link to the Creative Commons licence, and indicate if changes were made. The images or other third party material in this article are included in the article's Creative Commons licence, unless indicated otherwise in a credit line to the material. If material is not included in the article's Creative Commons licence and your intended use is not permitted by statutory regulation or exceeds the permitted use, you will need to obtain permission directly from the copyright holder. To view a copy of this licence, visit <http://creativecommons.org/licenses/by/4.0/>.

References

1. Kelley PE, Scholes MA (2007) Microtia and congenital aural atresia. *Otolaryngol Clin N Am* 40(1):61–80. <https://doi.org/10.1016/j.otc.2006.10.003>. Congenital Anomalies of the Head and Neck
2. Cabin JA, Bassiri-Tehrani M, Sclafani AP, Romo T (2014) Microtia reconstruction: autologous rib and alloplast techniques. *Facial Plast Surg Clin North Am* 22(4):623–638. <https://doi.org/10.1016/j.fsc.2014.07.004>
3. Luquetti DV, Leoncini E, Mastroiacovo P (2011) Microtia-ano-tia: A global review of prevalence rates. *Birth Defects Res A* 91(9):813–822. <https://doi.org/10.1002/bdra.20836>
4. Cruz RLJ, Ross MT, Powell SK, Woodruff MA (2020) Advancements in soft-tissue prosthetics part a: The art of imitating life. *Frontiers in bioengineering and biotechnology* 8:121. <https://doi.org/10.3389/fbioe.2020.00121>
5. Tanner PB, Mobley SR (2006) External auricular and facial prosthetics: a collaborative effort of the reconstructive surgeon and anaplastologist. *Facial Plast Surg Clin North Am* 14(2):137–45, vi–vii. <https://doi.org/10.1016/j.fsc.2006.01.003>
6. Kozusko SD, Konofaos P, Wallace RD (2020) The history of alloplastic ear reconstruction for microtia. *Ann Plast Surg* 85(1):89–92. <https://doi.org/10.1097/SAP.0000000000002213>
7. Storck K, Staudenmaier R, Buchberger M, Strenger T, Kreutzer K, von Bomhard A, Stark T (2014) Total reconstruction of the auricle: Our experiences on indications and recent techniques. *Biomed Res Int* 373286:15. <https://doi.org/10.1155/2014/373286>
8. Cronin TD (1966) Use of a silastic frame for total and subtotal reconstruction of the external ear: Preliminary report. *Plast Reconstr Surg* 37(5)
9. Ring ME (1991) The history of maxillofacial prosthetics. *Plast Reconstr Surg* 87(1)
10. Paprocki GJ (2013) Maxillofacial prosthetics: history to modern applications. part 1 - obturators. *Compendium of continuing education in dentistry (Jamesburg, NJ : 1995)* 34(8):e84–6
11. Atay A (2013) Overview of maxillofacial prosthetics, vol 1, 1st edn. Nova Science Publishers Incorporated. (Accessed on: 20 April 2022). <https://novapublishers.com/shop/overview-of-maxillofacial-prosthetics/>
12. Nayyer L, Birchall M, Seifalian AM, Jell G (2014) Design and development of nanocomposite scaffolds for auricular reconstruction. *Nanomedicine: Nanotechnology, Biology and Medicine* 10(1):235–246. <https://doi.org/10.1016/j.nano.2013.06.006>
13. Federspil PA (2018) Auricular prostheses in microtia. *Facial Plast Surg Clin North Am* 26(1):97–104. <https://doi.org/10.1016/j.fsc.2017.09.007>
14. Artioli BO, Kunkel ME, Mestanza SN (2019) Feasibility study of a methodology using additive manufacture to produce silicone ear prostheses. In: *World Congress on Medical Physics and Biomedical Engineering 2018*. Springer, pp 211–215. https://doi.org/10.1007/978-981-10-9023-3_38

15. Rogati G, Leardini A, Ortolani M, Caravaggi P (2019) Validation of a novel kinect-based device for 3D scanning of the foot plantar surface in weight-bearing. *Journal of Foot and Ankle Research* 12(1):1–8. <https://doi.org/10.1186/s13047-019-0357-7>
16. Louis PJ, Aponte-Wesson RA, Fernandes RP, Clemow J (2013) Autogenous and prosthetic reconstruction of the ear. *Oral Maxillofac Surg Clin North Am* 25(2):271–286. <https://doi.org/10.1016/j.coms.2013.02.001>
17. Mussi E, Furferi R, Volpe Y, Facchini F, McGreevy KS, Uccheddu F (2019) Ear reconstruction simulation: from handcrafting to 3D printing. *Bioengineering* 6(1):14. <https://doi.org/10.3390/bioengineering6010014>
18. Manero A, Smith P, Sparkman J, Dombrowski M, Courbin D, Kester A, Womack I, Chi A (2019) Implementation of 3D printing technology in the field of prosthetics: Past, present, and future. *Int J Environ Res Public Health* 16(9):1641. <https://doi.org/10.3390/ijerph16091641>
19. He Y, Xue Gh, Jz Fu (2014) Fabrication of low cost soft tissue prostheses with the desktop 3D printer. *Sci Rep* 4(1):1–7. <https://doi.org/10.1038/srep06973>
20. Eggbeer D, Bibb R, Evans P, Ji L (2012) Evaluation of direct and indirect additive manufacture of maxillofacial prostheses. *Proc Inst Mech Eng [H]* 226(9):718–728. <https://doi.org/10.1177/0954411912451826>
21. Ferraz MdAMM, Nagashima JB, Venzac B, Le Gac S, Songsasen N (2020) 3D printed mold leachates in pdms microfluidic devices. *Sci Rep* 10(1):1–9. <https://doi.org/10.1038/s41598-020-57816-y>
22. Villegas M, Cetinic Z, Shakeri A, Didar TF (2018) Fabricating smooth PDMS microfluidic channels from low-resolution 3D printed molds using an omniphobic lubricant-infused coating. *Anal Chim Acta* 1000:248–255. <https://doi.org/10.1016/j.aca.2017.11.063>
23. Hwang Y, Paydar OH, Candler RN (2015) 3D printed molds for non-planar PDMS microfluidic channels. *Sensors and Actuators A: Physical* 226:137–142. <https://doi.org/10.1016/j.sna.2015.02.028>
24. Nag A, Feng S, Mukhopadhyay S, Kosel J, Inglis D (2018) 3D printed mould-based graphite/PDMS sensor for low-force applications. *Sensors and Actuators A: Physical* 280:525–534. <https://doi.org/10.1016/j.sna.2018.08.028>
25. Bonyár A, Sántha H, Ring B, Varga M, Kovács JG, Harsányi G (2010) 3D rapid prototyping technology (RPT) as a powerful tool in microfluidic development. *Procedia Engineering* 5:291–294. <https://doi.org/10.1016/j.proeng.2010.09.105>
26. Liravi F, Toyserkani E (2018) Additive manufacturing of silicone structures: A review and prospective. *Addit Manuf* 24:232–242. <https://doi.org/10.1016/j.addma.2018.10.002>
27. Melchels FP, Feijen J, Grijpma DW (2010) A review on stereolithography and its applications in biomedical engineering. *Biomaterials* 31(24):6121–6130. <https://doi.org/10.1016/j.biomaterials.2010.04.050>
28. Murphy SV, Atala A (2014) 3D bioprinting of tissues and organs. *Nat Biotechnol* 32(8):773–785. <https://doi.org/10.1038/nbt.2958>
29. Gibson I, Rosen D, Stucker B, Khorasani M (2014) Additive manufacturing technologies, vol 17. Springer
30. Jones N (2012) Science in three dimensions: the print revolution. *Nature News* 487(7405):22. <https://doi.org/10.1038/487022a>
31. Ross MT, Cruz R, Hutchinson C, Arnott WL, Woodruff MA, Powell SK (2018) Aesthetic reconstruction of microtia: a review of current techniques and new 3D printing approaches. *Virtual and Physical Prototyping* 13(2):117–130. <https://doi.org/10.1080/17452759.2018.1430246>
32. Mohammed MI, Tatineni J, Cadd B, Peart G, Gibson I (2017) Advanced auricular prosthesis development by 3D modelling and multi-material printing. In: *DesTech 2016: Proceedings of the International Conference on Design and Technology, Knowledge E*. pp 37–43. <https://doi.org/10.18502/keg.v2i2.593>
33. Mannoor MS, Jiang Z, James T, Kong YL, Malatesta KA, Soboyejo WO, Verma N, Gracias DH, McAlpine MC (2013) 3D printed bionic ears. *Nano Lett* 13(6):2634–2639. <https://doi.org/10.1021/nl4007744>
34. Haleem A, Javaid M (2019) 3D scanning applications in medical field: a literature-based review. *Clinical Epidemiology and Global Health* 7(2):199–210. <https://doi.org/10.1016/j.cegh.2018.05.006>
35. Abdullah A, Mohamad D, Din T, Yahya S, Akil H, Rajion Z (2019) Fabrication of nasal prosthesis utilising an affordable 3d printer. *Int J Adv Manuf Technol* 100(5–8):1907–1912. <https://doi.org/10.1007/s00170-018-2831-y>
36. Sohaib A, Amano K, Xiao K, Yates J, Whitford C, Wuerger S (2018) Colour quality of facial prostheses in additive manufacturing. *Int J Adv Manuf Technol* 96(1–4):881–894. <https://doi.org/10.1007/s00170-017-1480-x>
37. Huang X, Ye M, Zhang W, Wang C, Jiao T (2004) Fabricating auricular prostheses based on rapid prototyping and the freeform modelling system. *Int J Adv Manuf Technol* 24(11–12):873–878. <https://doi.org/10.1007/s00170-003-1814-8>
38. Sherwood R, Murphy N, Kearns G, Barry C (2020) The use of 3D printing technology in the creation of patient-specific facial prostheses. *Ir J Med Sci* 189(4):1215–1221. <https://doi.org/10.1007/s11845-020-02248-w>
39. Jain R, Mahendru S, Aggarwal A, Brajesh V, Aulakh H, Singh S, Jain A, Khazanchi R (2021) Feasibility of customised polymethyl methacrylate implants fabricated using 3d printed flexible moulds for correction of facial skeletal deformities. *J Craniofac Surg* 32(6):1981–1985. <https://doi.org/10.1097/SCS.00000000000007383>
40. Tanveer W, Ridwan-Pramana A, Molinero-Mourelle P, Koolstra J, Forouzanfar T (2021) Systematic review of clinical applications of CAD/CAM technology for craniofacial implants placement and manufacturing of nasal prostheses. *Int J Environ Res Public Health* 18(7). <https://doi.org/10.3390/ijerph18073756>
41. Miechowicz S, Wojnarowska W, Majkut S, Trybulec J, Pijanka D, Piecuch T, Sochacki M, Kudasik T (2021) Method of designing and manufacturing craniofacial soft tissue prostheses using additive manufacturing: A case study. *Biocybernetics and Biomedical Engineering* 41(2):854–865. <https://doi.org/10.1016/j.bbe.2021.05.008>
42. Rodrigues TA, Bairrao N, Farias FWC, Shamsolhodaie A, Shen J, Zhou N, Maawad E, Schell N, Santos TG, Oliveira J (2022) Steel-copper functionally graded material produced by twin-wire and arc additive manufacturing (T-WAAM). *Mater Des* 213:110270. <https://doi.org/10.1016/j.matdes.2021.110270>
43. Rodrigues TA, Duarte VR, Miranda R, Santos TG, Oliveira J (2021) Ultracold-wire and arc additive manufacturing (UC-WAAM). *J Mater Process Technol* 296:117196. <https://doi.org/10.1016/j.jmatprotec.2021.117196>
44. Robinson TM, Talebian S, Foroughi J, Yue Z, Fay CD, Wallace GG (2020) Fabrication of aligned biomimetic gellan gum-chitosan microstructures through 3D printed microfluidic channels and multiple in situ cross-linking mechanisms. *ACS Biomaterials Science & Engineering* 6(6):3638–3648. <https://doi.org/10.1021/acsbiomaterials.0c00260>
45. Lin YW, Tsou KL, Fay CD, Liu X, Chung JH, Sharma D, Jeiranikhameh A, Kuo PH, Tzeng CK, Wallace GG, Wu CY, Ker MD, Chao JI, Cheng YT (2020) A microvalve cell printing technique using riboflavin photosensitizer for selective cell patterning onto a retinal chip. *Bioprinting* 20:00097. <https://doi.org/10.1016/j.bprint.2020.e00097>
46. Nagle AR, Fay CD, Xie Z, Wallace GG, Wang X, Higgins MJ (2019b) A direct 3D suspension near-field electrospinning technique for the fabrication of polymer nanoarrays. *Nanotechnology* 30(19):195301. <https://doi.org/10.1088/1361-6528/ab011b>
47. Nagle AR, Fay CD, Wallace GG, Xie Z, Wang X, Higgins MJ (2019a) Patterning and process parameter effects in 3D suspension

- near-field electrospinning of nanoarrays. *Nanotechnology* 30(49):495301. <https://doi.org/10.1088/1361-6528/ab3c87>
48. Motas JG, Gorji NE, Nedelcu D, Brabazon D, Quadrini F (2021) XPS, SEM, DSC and nanoindentation characterization of silver nanoparticle-coated biopolymer pellets. *Appl Sci* 11(16). <https://doi.org/10.3390/app11167706>
49. Fay C (2020) Computer-Aided Design and Manufacturing (CAD/CAM) for Bioprinting, chap 3. Springer, pp 27–41
50. Chimene D, Lennox KK, Kaunas RR, Gaharwar AK (2016) Advanced bioinks for 3D printing: a materials science perspective. *Ann Biomed Eng* 44(6):2090–2102. <https://doi.org/10.1007/s10439-016-1638-y>
51. Heinrich G, Kaliske M, Lion A, Reese S (2009) Constitutive models for rubber VI. CRC Press
52. Grant GT, Liacouras PC (2017) Craniofacial applications of 3d printing. In: *3D Printing in Medicine*. Springer, pp 43–50
53. Yun WS, Shim JH, Park KH, Choi D, Park MI, Hwang SH, Kim SW et al (2018) Clinical application of 3-dimensional printing technology for patients with nasal septal deformities: a multicenter study. *JAMA Otolaryngology-Head & Neck Surgery* 144(12):1145–1152. <https://doi.org/10.1001/jamaoto.2018.2054>
54. Suh MK, Lee KH, Harijan A, Kim HG, Jeong EC (2017) Augmentation rhinoplasty with silicone implant covered with acellular dermal matrix. *Journal of Craniofacial Surgery* 28(2):445–448. <https://doi.org/10.1097/SCS.0000000000003225>

Publisher's Note Springer Nature remains neutral with regard to jurisdictional claims in published maps and institutional affiliations.